Supporting information

Double-mesoporous Core-shell Nanosystems based on Platinum Nanoparticles Functionalized with Lanthanide Complexes for *In Vivo* Magnetic Resonance Imaging and Photothermal Therapy

Lei Zhao[a], Xiaoqian Ge[a], Guihua Yan[b], Xiao Wang[c], Pengfei Hu[d], Liyi Shi[a], Otto S. Wolfbeis[e], Hongjie Zhang[c], and Lining Sun*[a]

[a] *Research Center of Nano Science and Technology, School of Material Science and Engineering, Shanghai University, Shanghai 200444, China. E-mail: lnsun@shu.edu.cn; Tel: +86-21-66137153*

[b] *Institute of Nanochemistry and Nanobiology, Shanghai University, Shanghai 200444, China.*

[c] *State Key Laboratory of Rare Earth Resource Utilization, Changchun Institute of Applied Chemistry, Chinese Academy of Sciences, Changchun 130022, China.*

[d] *Instrumental Analysis & Research Center, Shanghai University, Shanghai 200444, China.*

[e] *Institute of Analytical Chemistry, Chemo- and Biosensors, University of Regensburg, 93040 Regensburg, Germany.*

Calculation of the photothermal conversion efficiency

As follows, the photothermal conversion efficiency (η) of mPt@mSiO$_2$-GdDTPA nanosystems was calculated according to the previous reported methods[1].

$$\eta = \frac{hs(T_{max} - T_{max,H2O})}{I(1 - 10^{-A_{808}})}$$

(1)

Where *h* is heat transfer coefficient, *S* is the surface area of the container, T_{max} is the equilibrium temperature of mPt@mSiO$_2$-GdDTPA nanosystems, $T_{max,H2O}$ is the equilibrium temperature of water. *I* is the output power of 808 nm laser. And A_{808} is the absorption intensity of mPt@mSiO$_2$-GdDTPA nanosystems at 808 nm. The value of *hS* is derived according to eq 2,3,4:

We introduced a system time constant τ_s and a dimensionless term θ, they were defined as:

$$\theta = \frac{T - T_{surr}}{(T_{max} - T_{surr})}$$

(2)

$$\tau_s = \frac{\sum_i m_i C_{p,i}}{hs}$$

(3)

$$t = -\tau_s ln\theta \quad (4)$$

hs can be calculated from equation 3 and the unit is mW/°C (with τ_s = 188.53 s, *m* = 0.44 g, *C* = 4.2 J/g). Substituting *I* = 1.5 W, A_{808} = 0.30, $T_{max} - T_{max,H2O}$ = 21.2 °C to equation 1, the photothermal conversion efficiency (η) of mPt@mSiO$_2$-GdDTPA nanosystems was calculated to be 27%.

References

1. X. Q. Ge, Z. M. Song, L. N. Sun, Y. F. Yang, L. Y. Shi, R. Si, W. Ren, X. E. Qiu,

and H. F. Wang, *Biomaterials,* 2016, **108**, 35-43.

2. X. Ding, C. H. Liow, M. Zhang, R. Huang, C. Li, H. Shen, M. Liu, Y. Zou, N. Gao, Z. Zhang, Y. Li, Q. Wang, S. Li, and J. Jiang, *J. Am. Chem. Soc.,* 2014, **136**, 15684−15693.

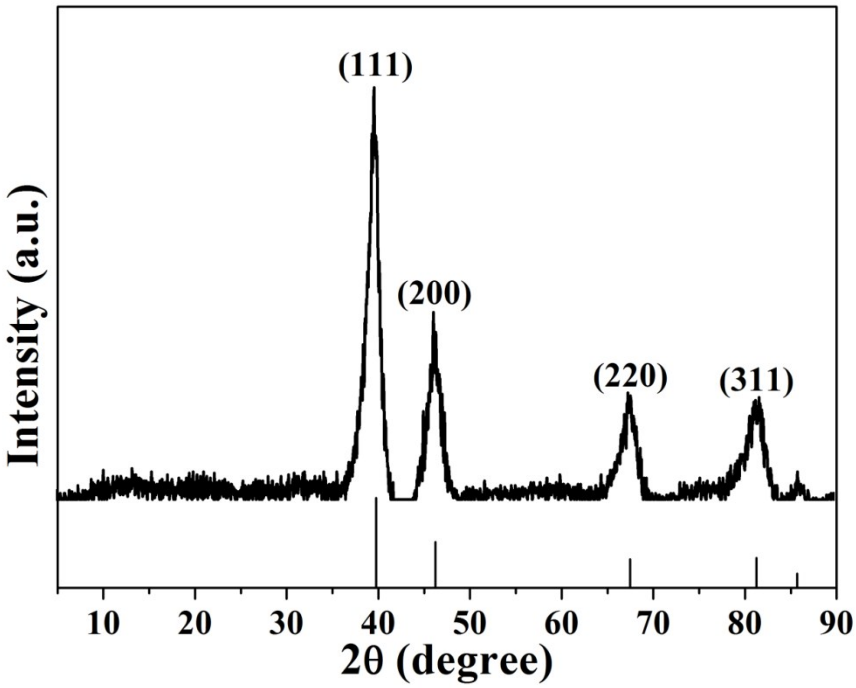

Fig. S1. X-ray diffraction pattern of mesoporous Pt nanoparticles (mPt NPs), and cubic phase JCPDS NO. 65-2868.

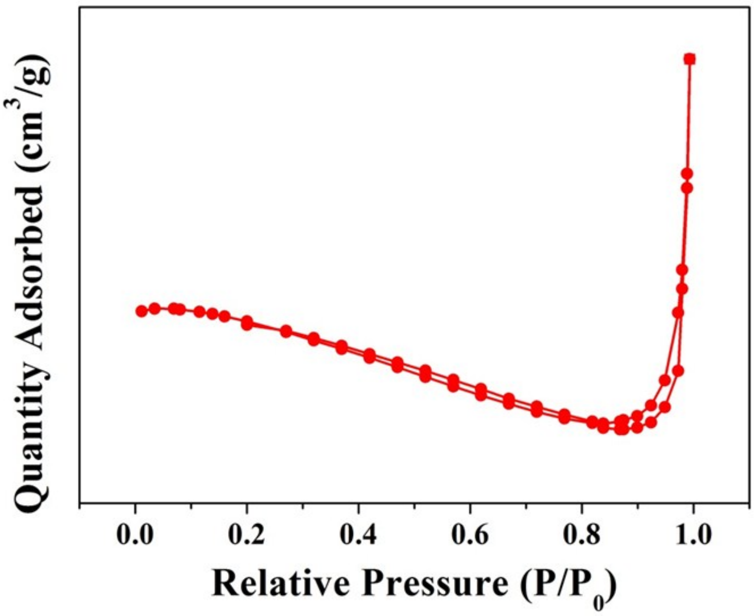

Fig. S2. N_2 adsorption/desorption isotherm of mPt NPs.

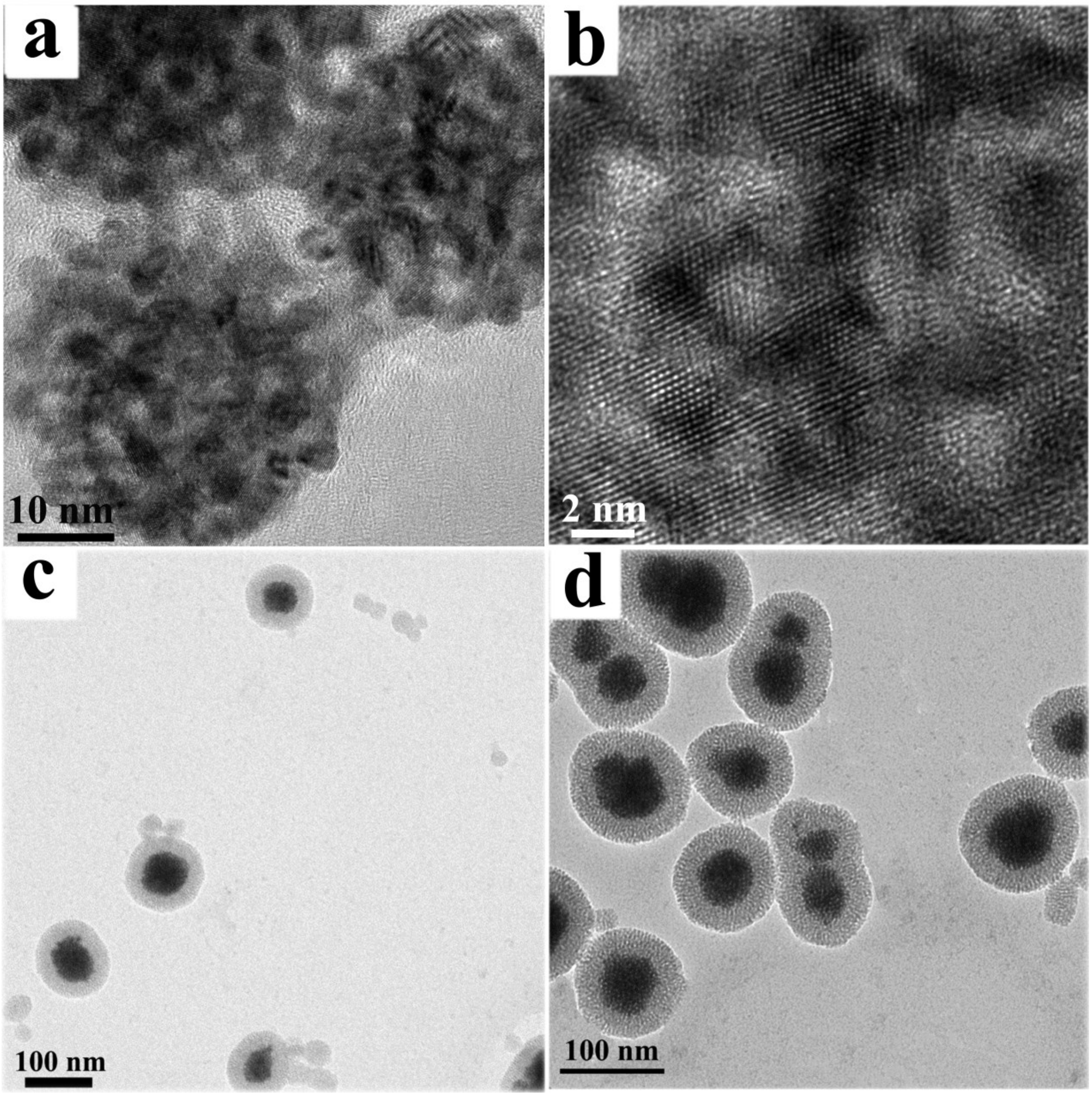

Fig. S3. High-resolution transmission electron microscope (HRTEM) images of mPt NPs (a and b)**;** Transmission electron microscope (TEM) images of mPt@mSiO_2 (c) and mPt@mSiO_2-GdDTPA (d).

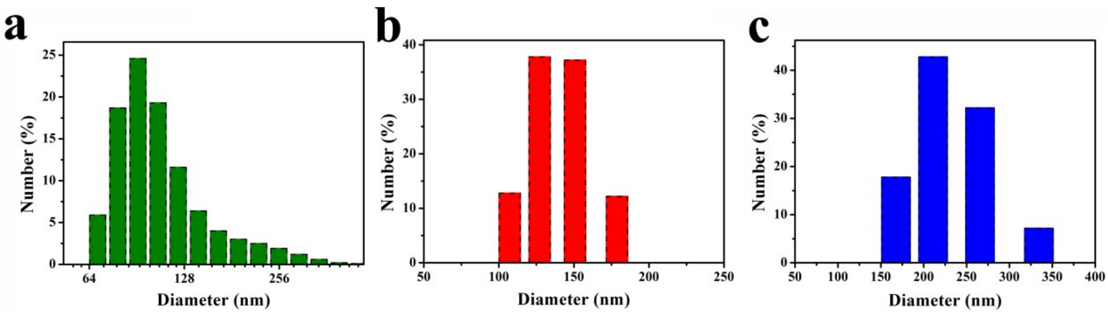

Fig. S4. Dynamic Light Scattering (DLS) of mPt in PBS (a) and mPt in water (b), and DLS of mPt@mSiO$_2$-GdDTPA in water (c). The polydispersity index (PDI) of Fig. S4 a-c is 0.39, 0.14, and 0.09, respectively.

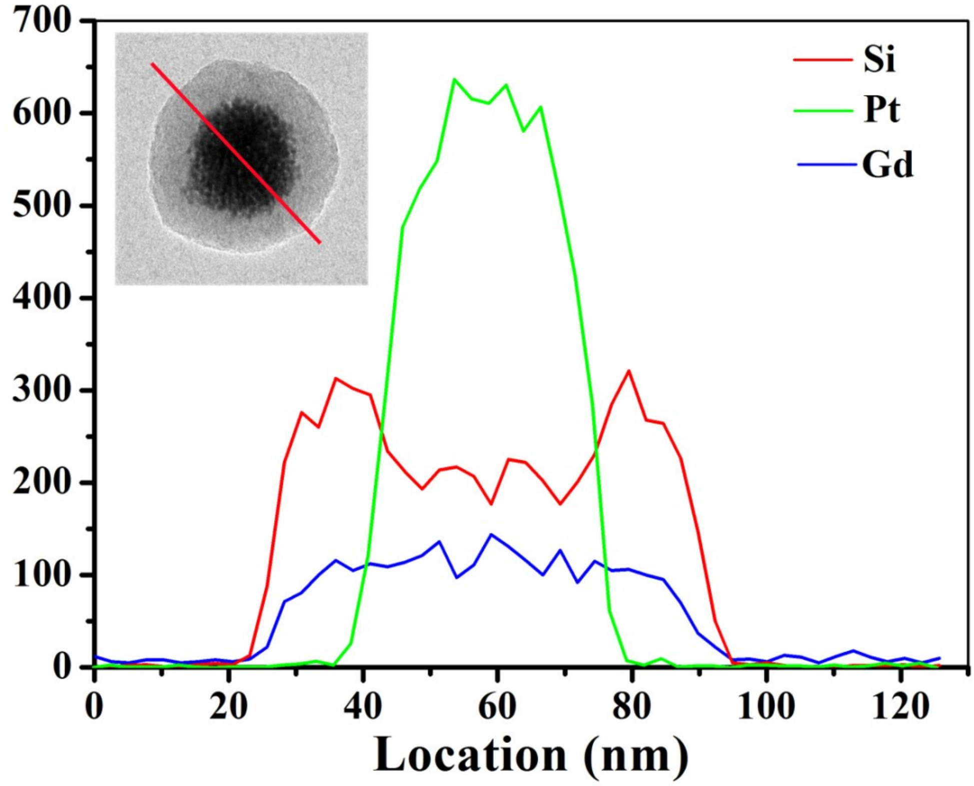

Fig. S5. The linear distribution of Si, Pt, and Gd elements in mPt@mSiO_2-GdDTPA.

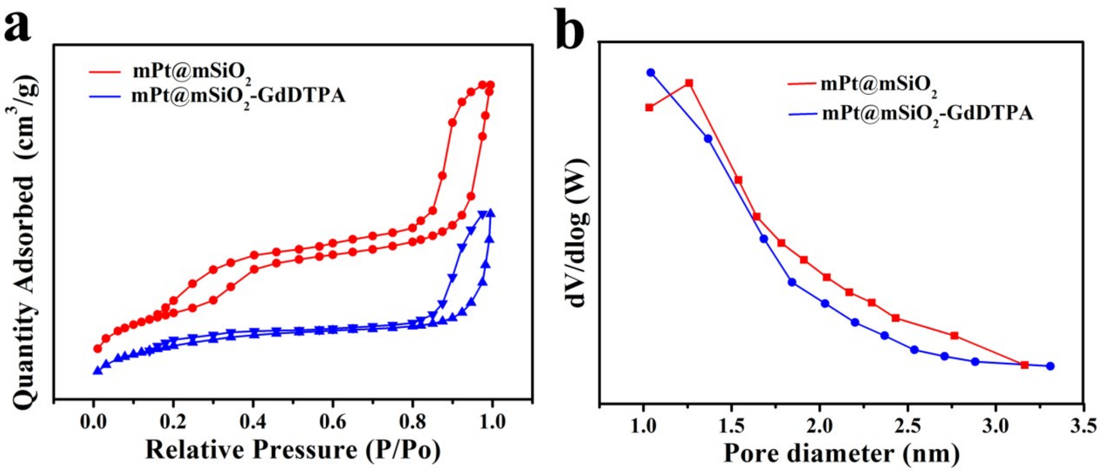

Fig. S6. N_2 adsorption/desorption isotherms of mPt@mSiO_2 and mPt@mSiO_2-GdDTPA (a); Pore size distributions of mPt@mSiO_2 and mPt@mSiO_2-GdDTPA (b).

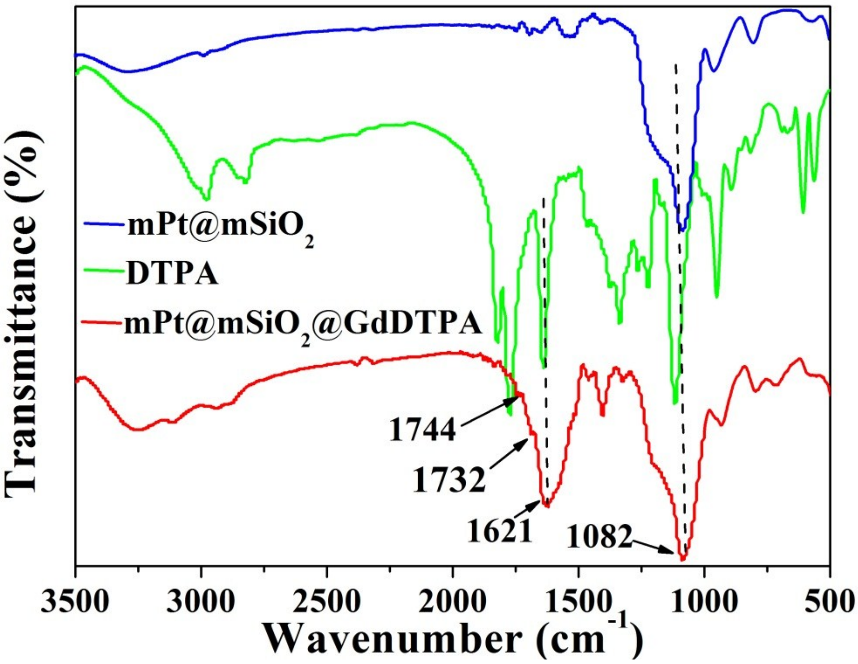

Fig. S7. FTIR spectra of mPt@mSiO$_2$-GdDTPA, mPt@mSiO$_2$, and DTPA.

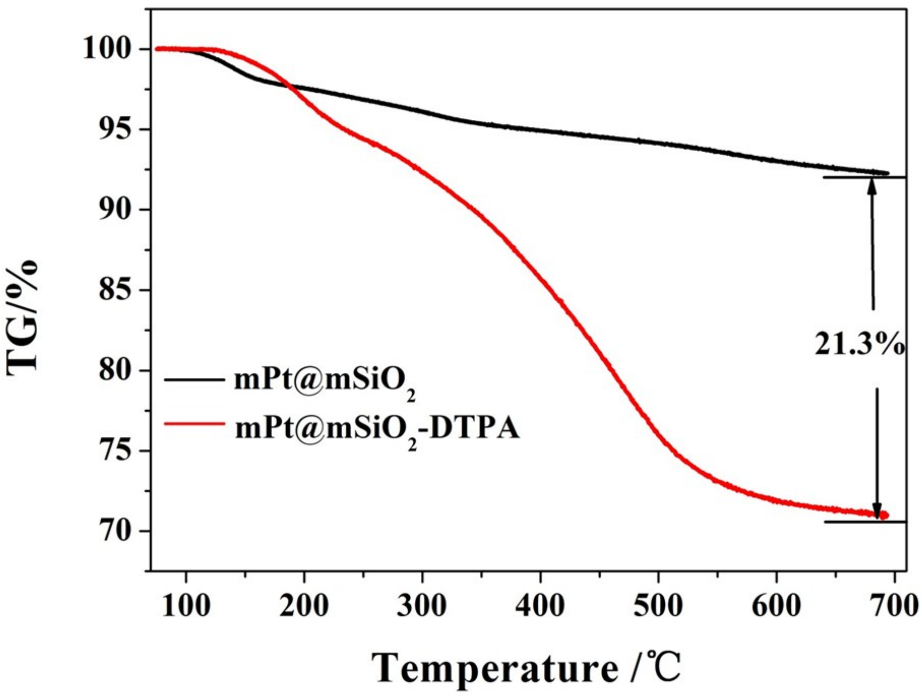

Fig. S8. The thermogravimetric curves of mPt@mSiO_2 and mPt@mSiO_2-DTPA.

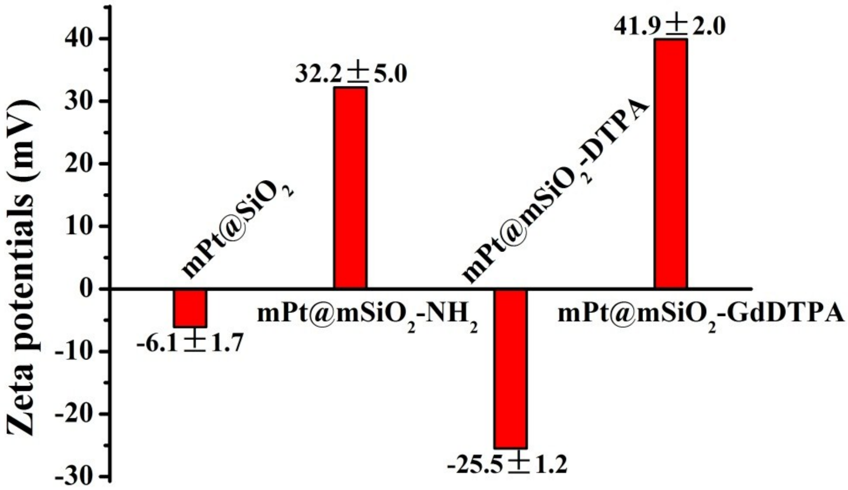

Fig. S9. The zeta potentials of mPt@SiO_2, mPt@SiO_2-NH_2, mPt@SiO_2-DTPA, and mPt@SiO_2-GdDTPA.

Table. S1. The zeta potentials of $mPt@SiO_2$, $mPt@SiO_2$-NH_2, $mPt@SiO_2$-DTPA, and $mPt@SiO_2$-GdDTPA in water.

Sample	**Zeta potential (mV)**
$mPt@SiO_2$	-6.1 ± 1.7
$mPt@SiO_2$-NH_2	32.2 ± 5.0
$mPt@SiO_2$-DTPA	-25.5 ± 1.2
$mPt@SiO_2$-GdDTPA	41.9 ± 2.0

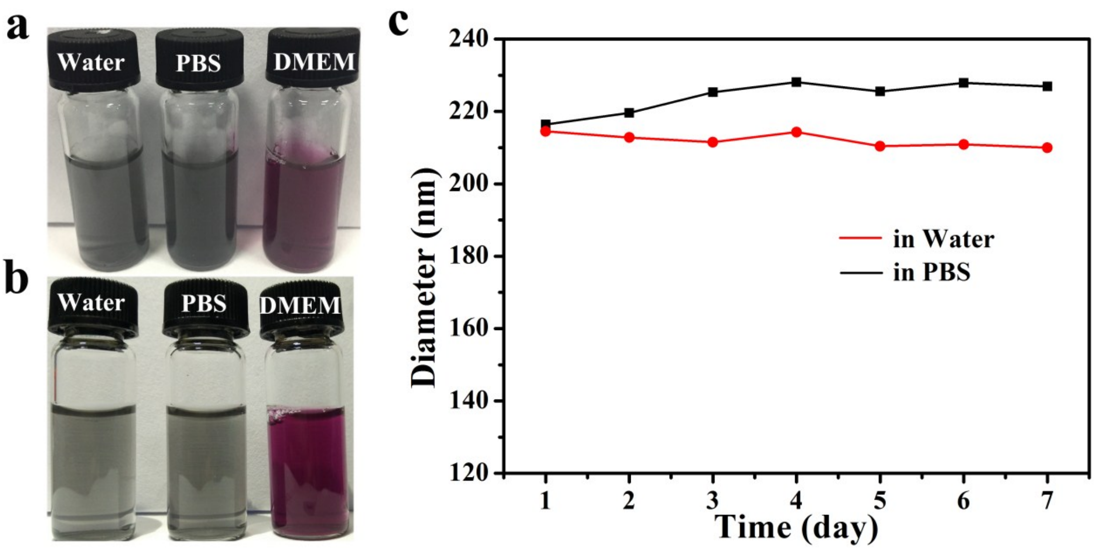

Fig. S10. The photos of mPt@mSiO_2-GdDTPA in water, PBS (pH = 7.4) and DMEM culture solution (a), and after being placed in the lab at room temperature for one week (b), and the DLS sizes of mPt@mSiO_2-GdDTPA during one week (c).

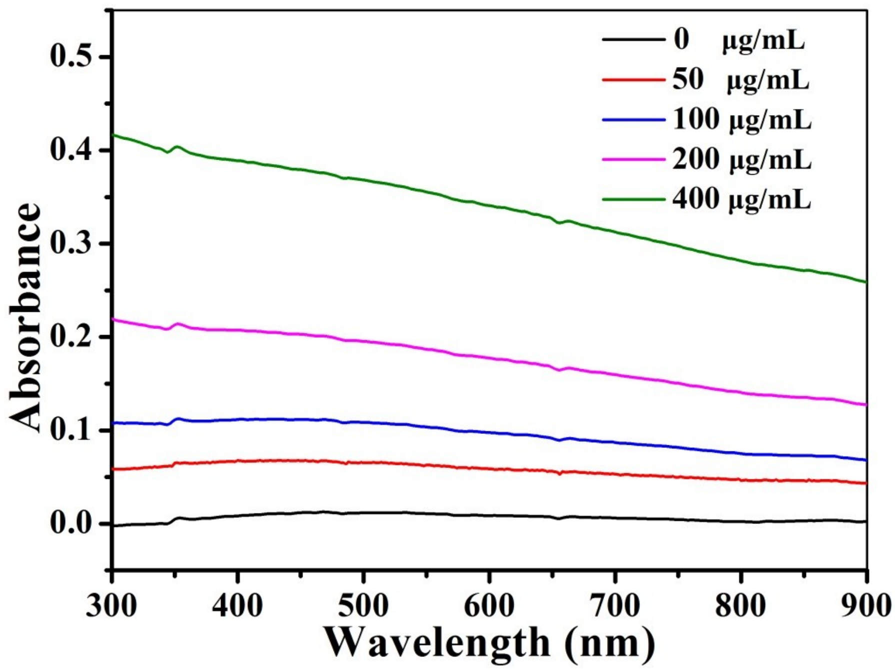

Fig. S11. UV-Vis-NIR absorption spectra of different concentrations of mPt@mSiO$_2$-GdDTPA in water.

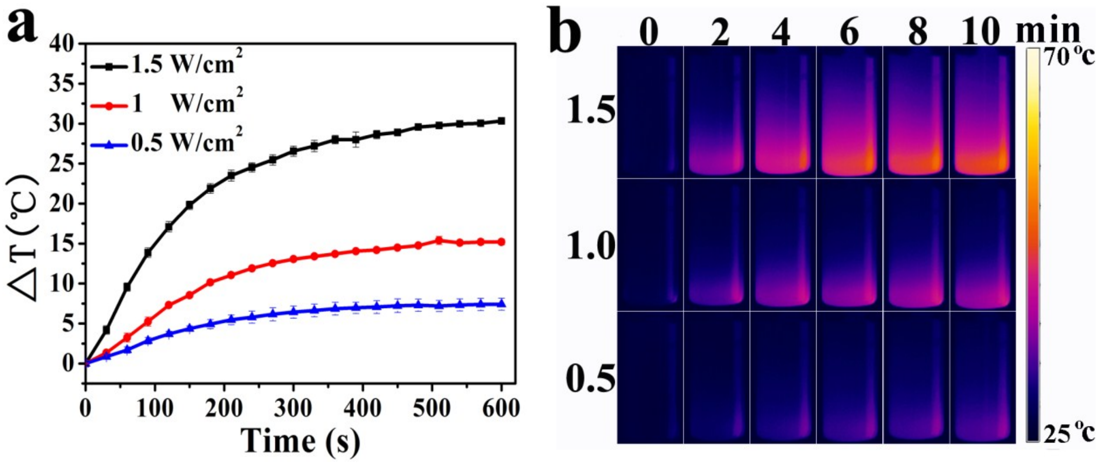

Fig. S12. Temperature changes (a) and infrared thermal images (b) of mPt@mSiO_2-GdDTPA (400 μg/mL) under 808 nm laser irradiation for 10 min with different power (1.5 W/cm^2, 1 W/cm^2, 0.5 W/cm^2).

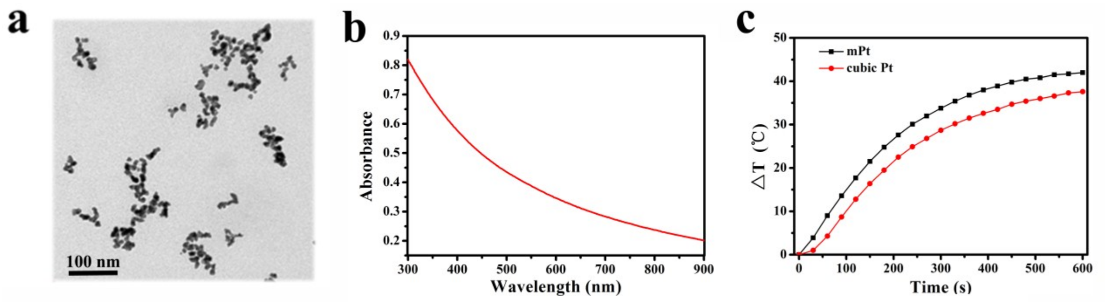

Fig. S13. Transmission electron microscope (TEM) image of cubic Pt NPs (a); UV-Vis-NIR absorption spectrum of cubic Pt NPs in water (b); Temperature changes of mPt NPs and cubic Pt NPs (60 μg/mL) under 808 nm laser irradiation for 10 min (1.5 W/cm^2) (c).

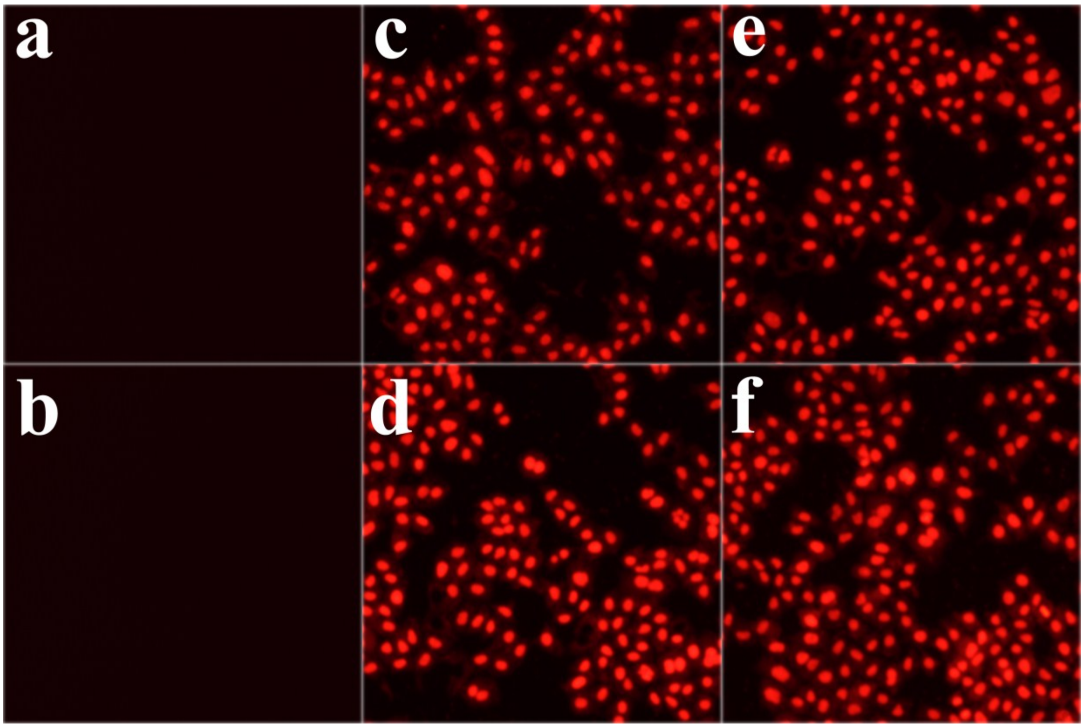

Fig. S14. Inverted fluorescence microscope of HeLa cells stained with PI based on laser illumination 808 nm laser; control group without laser (a), control group with laser (2 W/cm^2, 15 min) (b), sample with 1.5 W/cm^2 laser for 10 min (c), and 15 min (d), and sample with 2 W/cm^2 laser for 10 min (e), and 15 min (f).

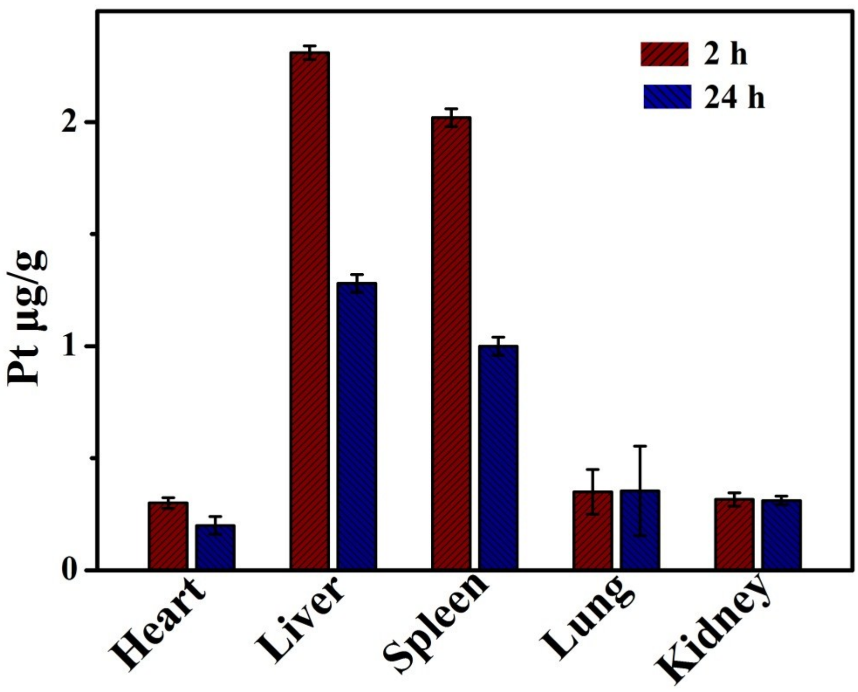

Fig. S15. Distributions of Pt in different organs of Kunming mice at 2 and 24 h post-injection of mPt@mSiO_2-GdDTPA NPs (n = 3, dose = 3 mg/mL).

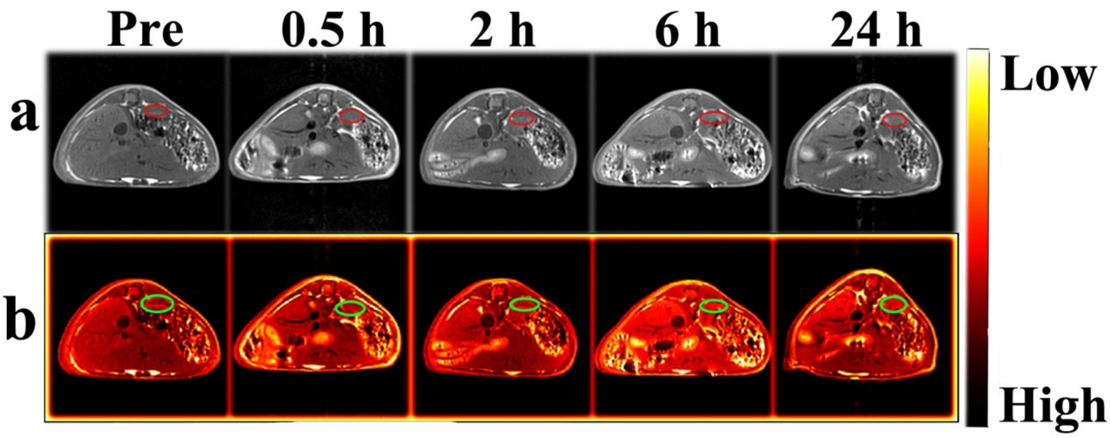

Fig. S16. *In vivo* T_1-weighted MR images of Kunming mice after the tail intravenous injection for varied time periods of spleen at the same dosage (3 mg/mL, 200 μL). The coronal images (a) and color mapped images (b). The red and green circles represent the region of spleen.